Supporting information

Effective enhancement the capacitive performance by means of facile exfoliation of bulk metal-organic frameworks into 2D functionalized nanosheets

Tianxiang Zheng, Xiaomin Kang*, Zhiliang Liu

Inner Mongolia Key Laboratory of Chemistry and Physics of Rare Earth Materials, College of Chemistry and Chemical Engineering, Inner Mongolia University, Hohhot, 010021, PR China. E-mail: kangxm@imu.edu.cn, E-mail: cezlliu@imu.edu.cn

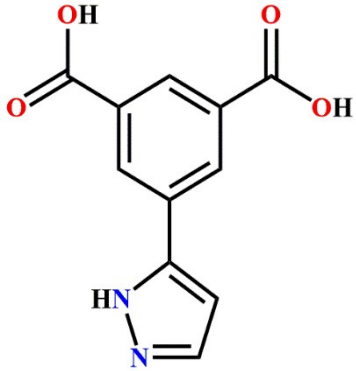

Scheme S1. The structure of H_2PIA ligand.

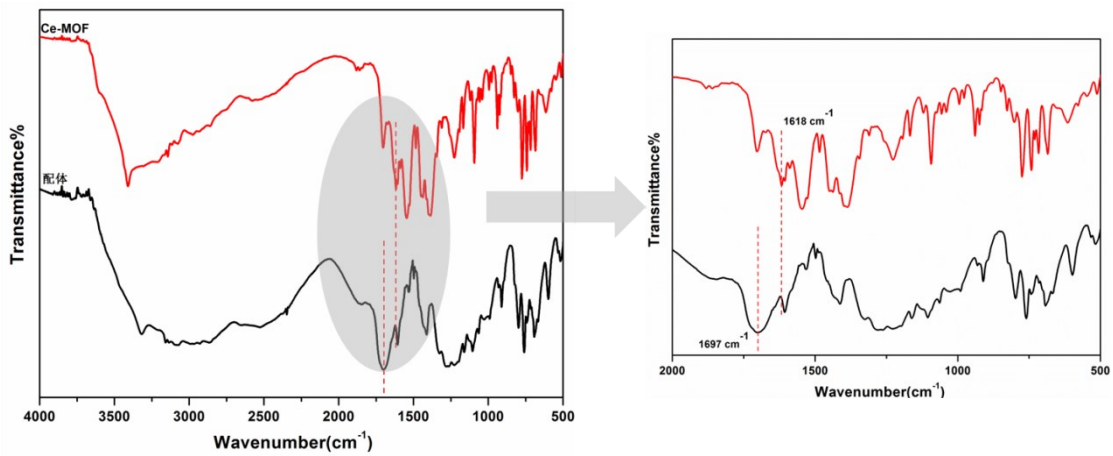

Fig. S1 IR spectrum of as-prepared Ce-MOF.

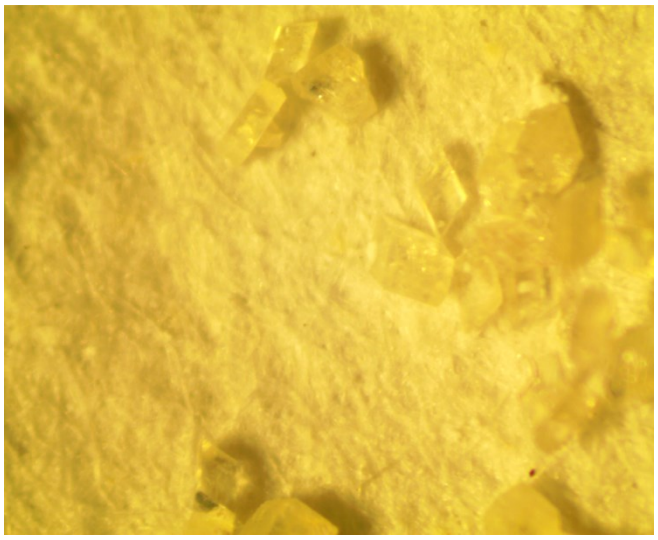

Fig. S2 Optical morphology of Ce-MOF crystal.

Table S1 Crystal data and structure refinement parameters of Ce-MOF.

Compound	Ce-MOF
Empirical formula	$C_{22}H_{19}CeN_4O_{11}$
Formula weight	655.51
Temperature/K	273.15
Crystal system	Triclinic
Space group	*P*-1
a/Å	9.3959(18)
b/Å	10.604(2)
c/Å	13.407(3)
α/°	97.634(2)
β/°	101.520(2)
γ/°	114.601(2)
Volume/Å^3	1154.7(4)
Z	2
ρ_{calc}g/cm^3	1.831
μ/mm^{-1}	2.038
F (000)	650
2θ range for data collection/°	6.4 to 56.7
Reflections collected	16339
R_{int}	0.0152
Goodness-of-fit on F^2	1.176
Final *R* indexes [I>=2σ (I)]	R_1 = 0.0247, wR_2 = 0.0701
Final *R* indexes [all data]	R_1 = 0.0252, wR_2 = 0.0706
$\Delta\rho_{max/min}$ (e Å^{-3})	0.98 and -0.82

Table S2 Selected bond lengths [Å] and angles [°] for Ce-MOF.

Bond lengths [Å]			
Ce(1)-O(4)	2.3638(19)	Ce(1)-O10	2.564(2)
Ce(1)-O(1)#1	2.4837(19)	O(1)-Ce(1)#1	2.4837(19)
Ce(1)-O(2)#2	2.4632(19)	O(2)-Ce(1)#4	2.4632(19)
Ce(1)-O(3)#3	2.4624(19)	O(3)-Ce(1)#3	2.4624(19)
Ce(1)-O(8)#3	2.5929(19)	O(8)-Ce(1)#3	2.5929(19)
Ce(1)-O(7)#3	2.5686(18)	O(7)-Ce(1)#3	2.5686(18)
Ce(1)-O9	2.5236(19)		

#1:2-X，3-Y，1-Z，#2:-1+X，-1+Y，+Z， #3:2-X，2-Y，1-Z;，#4:1+X，1+Y，+Z

Angles [°]			
O(4)-Ce(1)-O(3)#3	150.22(7)	O(3)#3-Ce(1)-O(1)#1	142.77(8)
O(4)-Ce(1)-O(8)#3	77.21(7)	O(3)#3-Ce(1)-O(2)#2	72.66(7)
O(4)-Ce(1)-O(7)#3	127.07(7)	O(3)#3-Ce(1)-O(8)#3	73.65(7)
O(4)-Ce(1)-O(9)	80.86(7)	O(3)#3-Ce(1)-O(7)#3	71.46(7)
O(4)-Ce(1)-O(10)	71.95(8)	O(3)#3-Ce(1)-O(9)	139.56(8)
O(1)#1-Ce(1)-O(8)#3	76.50(6)	O(3)#3-Ce(1)-O(10)	74.14(9)
O(1)#1-Ce(1)-O(7)#3	72.53(6)	O(7)#3-Ce(1)-O(8)#3	50.60(6)
O(1)#1-Ce(1)-O(9)	75.80(7)	O(9)-Ce(1)-O(8)#3	144.67(7)
O(1)#1-Ce(1)-O(10)	142.89(8)	O(9)-Ce(1)-O(7)#3	136.42(6)
O(2)#2-Ce(1)-O(1)#1	113.46(7)	O(9)-Ce(1)-O(10)	69.96(8)

#1:2-X，3-Y，1-Z，#2:-1+X，-1+Y，+Z， #3:2-X，2-Y，1-Z;，#4:1+X，1+Y，+Z

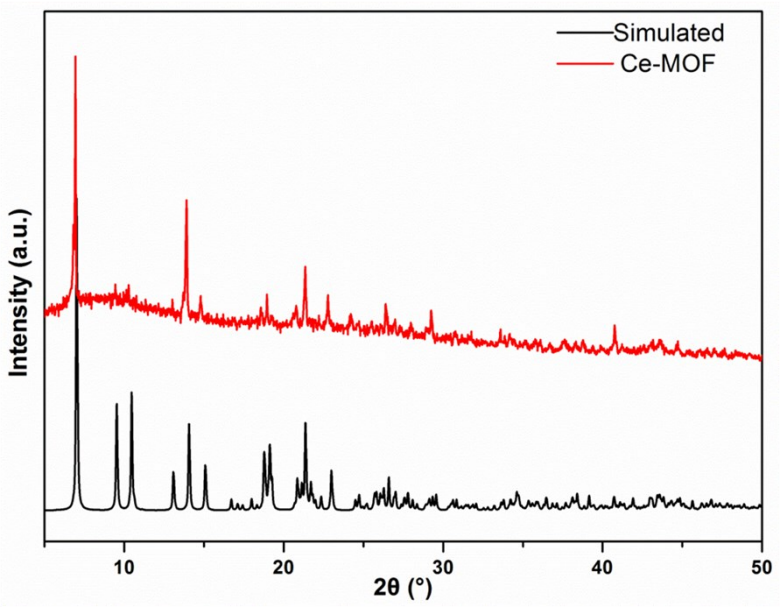

Fig. S3 The PXRD patterns for the simulated and experimental samples for Ce-MOF.

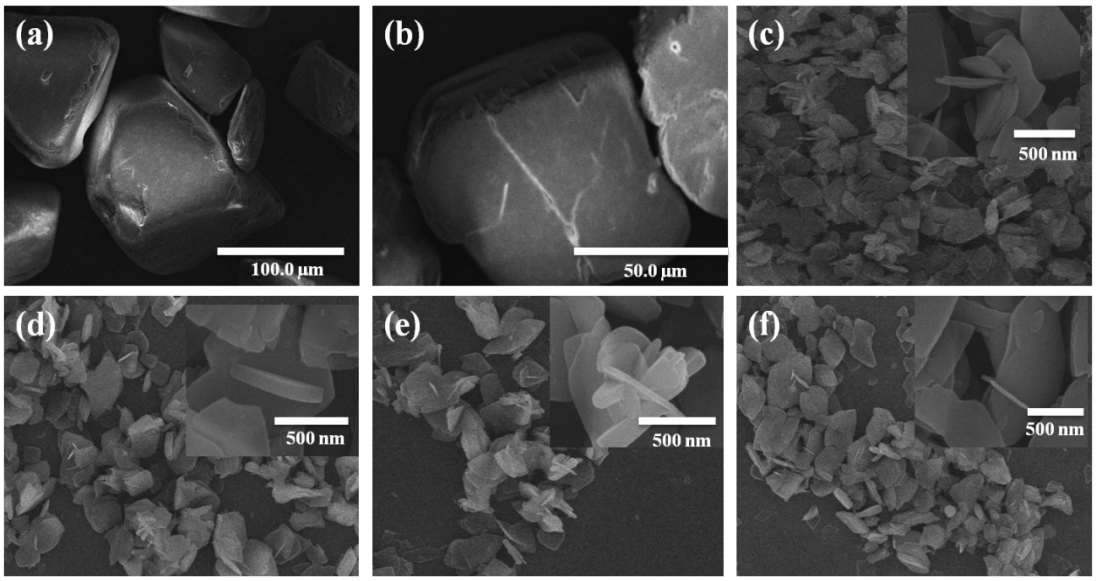

Fig. S4 The SEM images of Ni@Ce-MOF nanosheets after different reaction time.

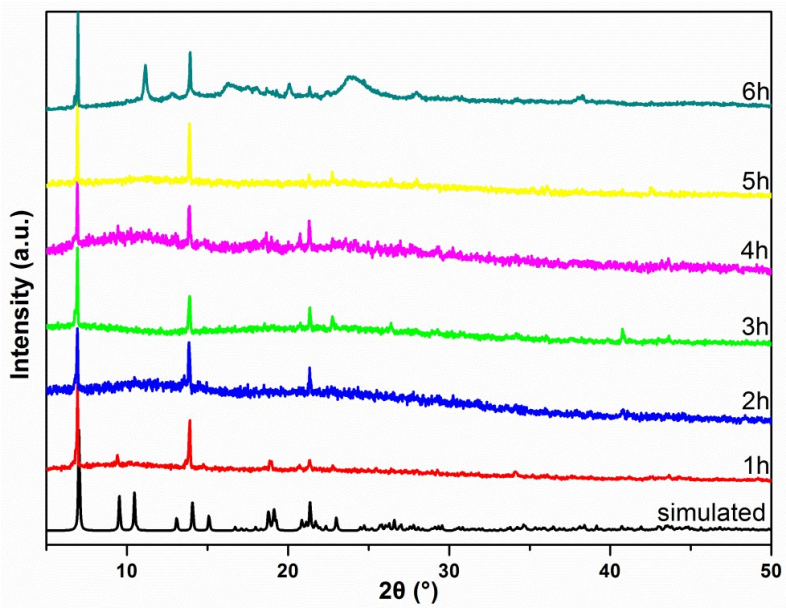

Fig. S5 The PXRD patterns for the simulated sample and Ni@Ce-MOF nanosheets after different reaction time.

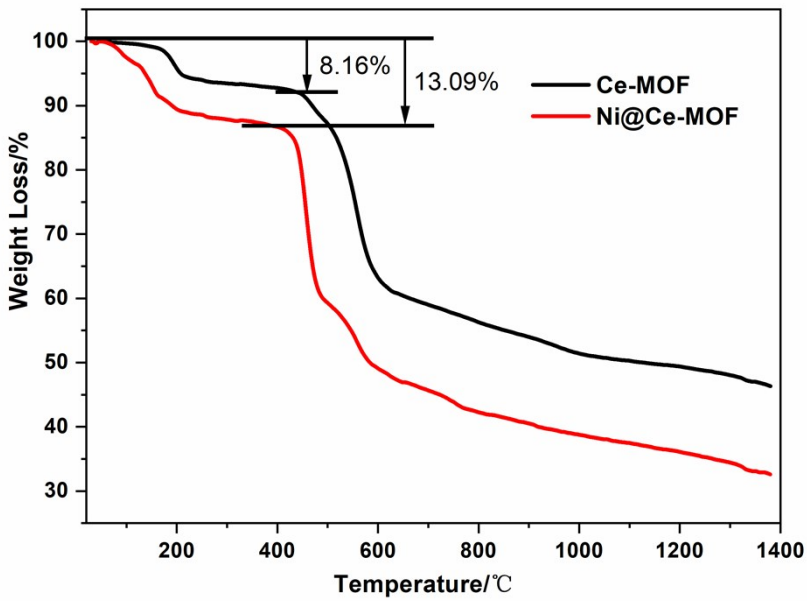

Fig. S6 The TGA curves of Ni@Ce-MOF and Ce-MOF, respectively.

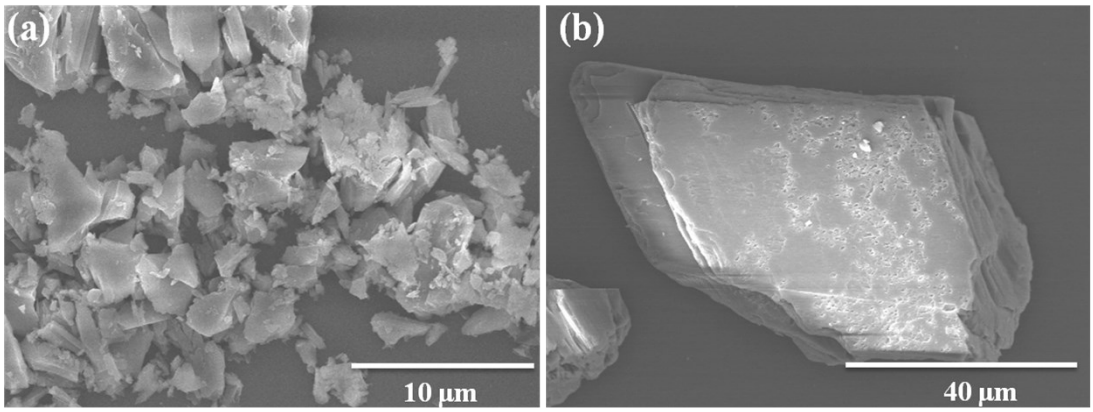

Fig. S7 The SEM images of blank **1** and blank **2**, respectively.

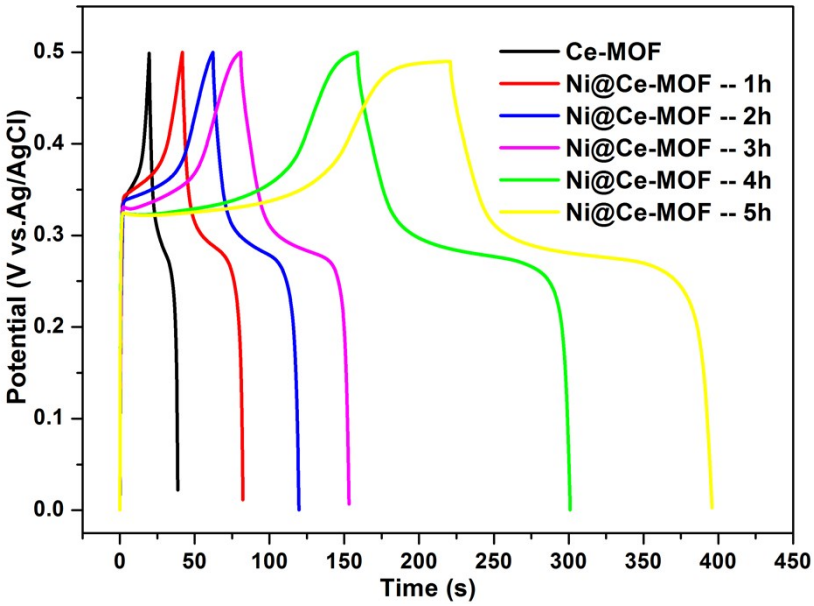

Fig. S8 The GCD curves for Ce-MOF and Ni@Ce-MOF nanosheets at 1 A g^{-1}, respectively.

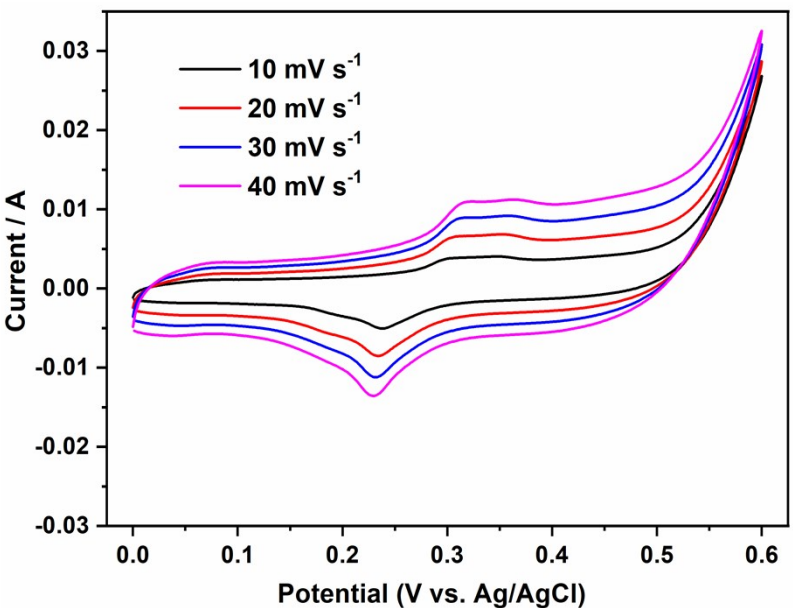

Fig. S9 The CV curves of Co^{2+}@Ce-MOF-5h nanosheets electrodes at different scan rates.

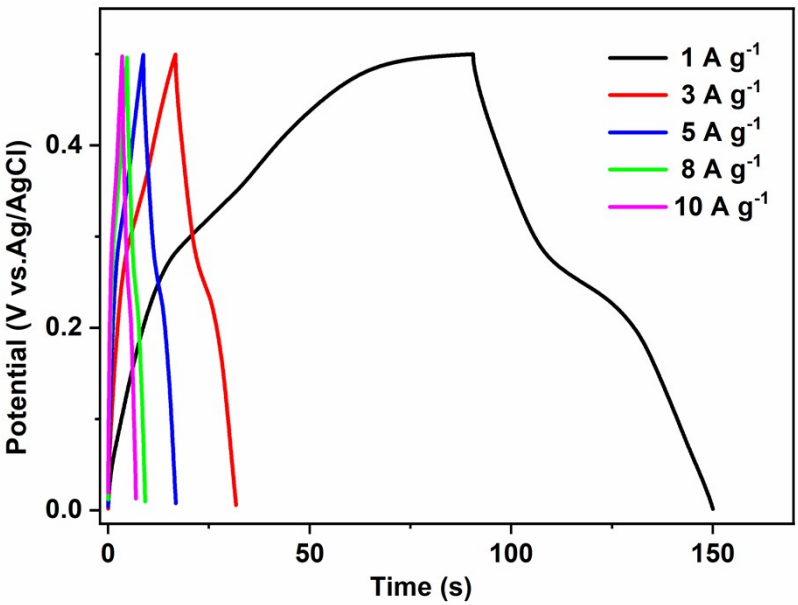

Fig. S10 The GCD curves of ASC (Co^{2+}@Ce-MOF-5h).

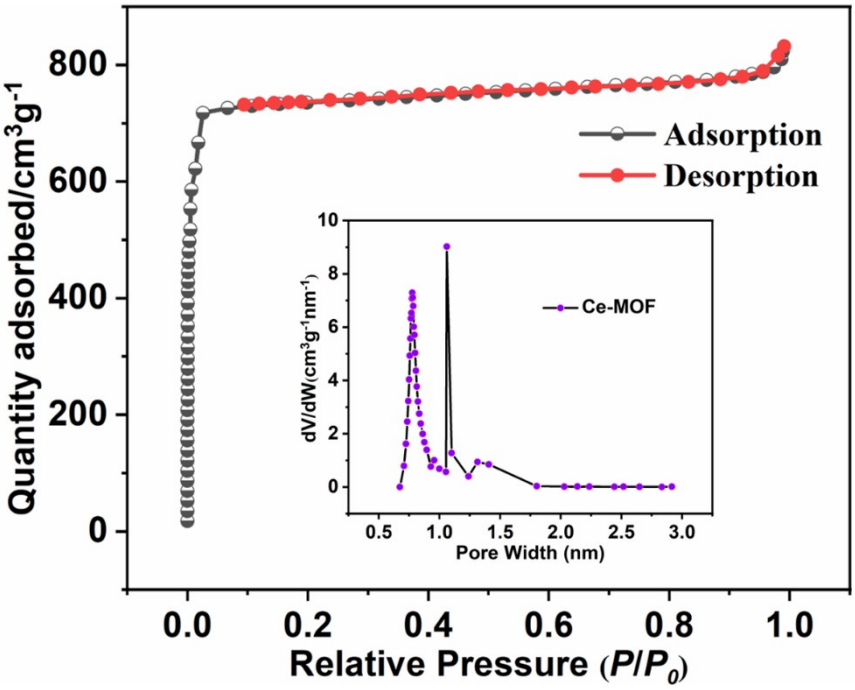

Fig. S11 The N_2 adsorption/desorption and pore distribution (insert) of Ce-MOF at 298 K.

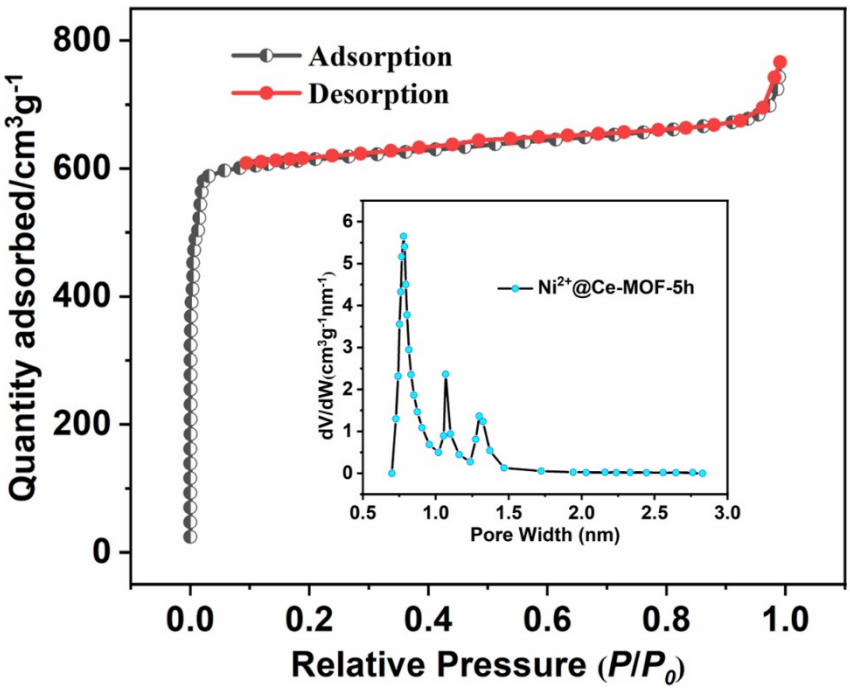

Fig. S12 The N_2 adsorption/desorption and pore distribution (insert) of Ni^{2+}@Ce-MOF-5h at 298 K.